

Planar Contactless Charging System Applying Three-Phase Power Transformer*

Hirokazu MATSUMOTO**, Yasuhiko NEBA**, Kouichi ISHIZAKA** and Ryozo ITOH**

This paper proposes a planar contactless charging system applying three-phase power transformer. The three-phase system has the capability of stable power transfer from the primary armature as a charging platform to the secondary armature as a mover with battery. This operation principle is different from the conventional planar contactless charging system, which applies the single-phase power transformer. Moreover, the arrangement of the windings for the three-phase system is proposed. The simulation results give that the proposed arrangement can generate the moving magnetic field with the stable amplitude at any time. The experiments using a prototype with the proposed arrangement prove that the three-phase system can stably transfer power independently of the position of the secondary armature.

Key Words : Contactless power transfer, moving magnetic field, planar charging system, printed circuit board (PCB), three-phase transformer.

I. INTRODUCTION

Considering easy and simple effort to charge movers, which have a wide variety of the power capacity from people movers to electric cars, contactless power transfer systems are the interesting charging systems because they can charge the movers as they are physically separated from the charging platform. Various contactless power transfer systems have been researched [1]-[7]. The planar charging system is one of the promising systems in the contactless power transfer systems [4]. This system can be used to transfer power to people movers with relatively low power, for example, cellphone, music player, laptop personal computer and so on, or to charge their batteries by just putting them on the charging platform, independently of their shape.

The planar charging system typically has the array of the coreless windings made of copper foil on a printed circuit board (PCB). This structure allows the planar systems to be manufactured easily and be realized in thin shape. Moreover, the planar system does not require the precision of the position of a secondary armature as a mover with batteries, for a primary armature as a charging platform to transfer power to the mover. In order to achieve the stable power transfer independent of the position of the secondary armature, the primary armature needs to produce uniform magnetic field distribution. The coreless windings have a spiral structure

to obtain as many turns as possible. This winding structure causes the nonuniform distribution, which has a peak value at the center of the winding and a valley value along the outer edge. The nonuniform distribution can be suppressed by employing the array of multiple windings with relatively small outer diameter. Furthermore, the winding array constructed in double or more layers can smooth the nonuniform distribution [4], [8]-[10]. To be specific, the windings are arranged as the center of the windings in a layer locates along the outer edge of the windings in the other layer [4], [9], [10]. Planar systems with various structures such as square and hexagon and arrangements of the windings have been reported to achieve the stable power transfer.

This paper proposes a planar contactless charging system with a novel concept basing on three-phase power transformer. According to [7], the three-phase system has the capability of the stable power transfer. The operation principle of the proposed system is the different from that of the conventional planar charging system, which applies the single-phase contactless power transformer. In the three-phase system, the moving magnetic field contributes to the stable power transfer. The principle for the three-phase system to generate the moving magnetic field is explained. Moreover, this paper proposes an arrangement of the windings for the three-phase planar charging system. The simulations using Bio-Savart's Law confirm that the armature with the proposed arrangement can generate sufficiently effective moving magnetic field, which has alternating distribution with almost

* Manuscript received Dec. 3, 2010.

** Department of Electrical engineering

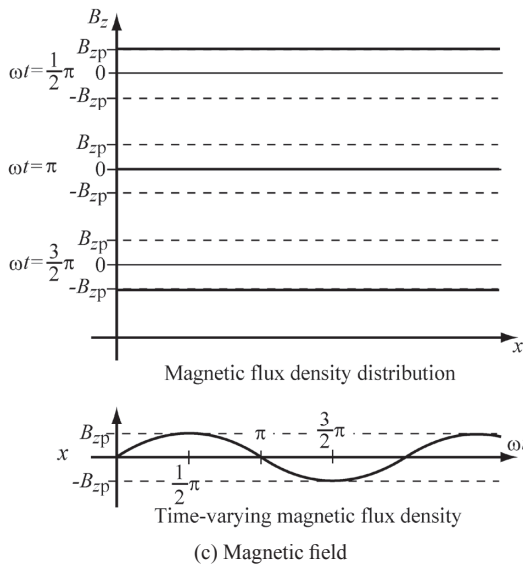
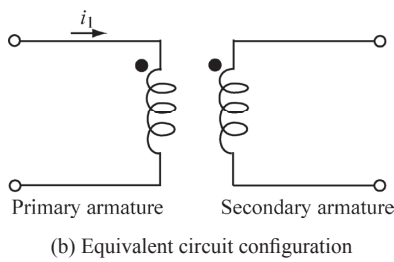
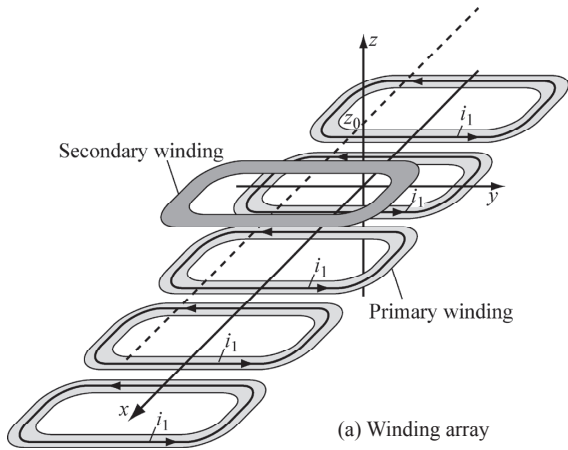


Fig.1 Single-phase planar contactless charging system

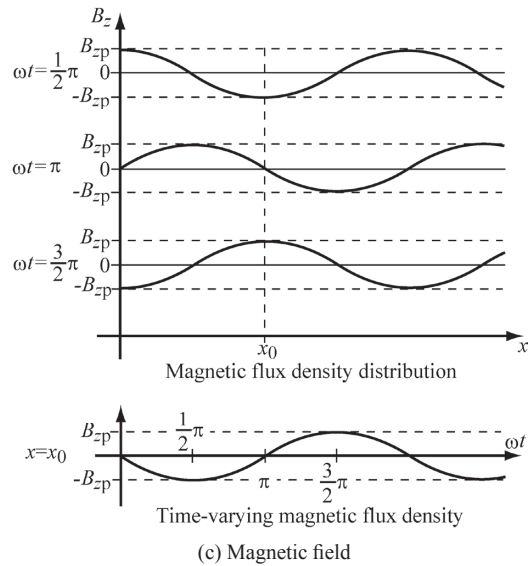
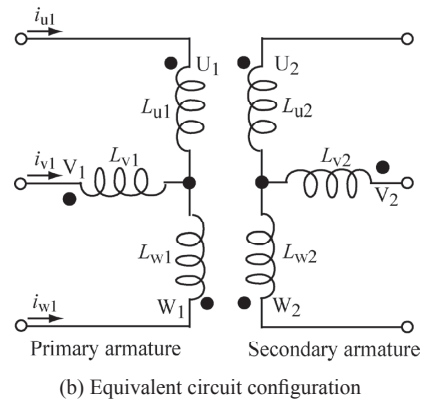
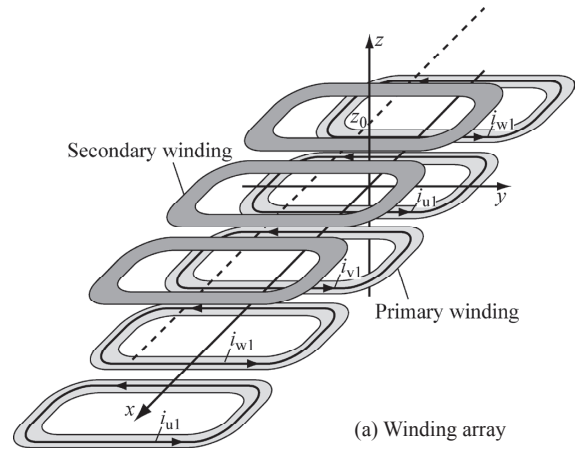


Fig.2 Three-phase planar contactless charging system

constant amplitude at any time. Finally, the experiments using a prototype of the three-phase planar charging system prove to be able to transfer stable power independent of the position of the secondary armature.

II. OPERATION PRINCIPLE OF THREE-PHASE PLANAR CONTACTLESS CHARGING SYSTEM

A. Difference from single-phase system

Fig. 1(a) shows a conventional single-phase planar contactless charging system. In the primary armature, the multiple windings are arrayed regularly. The secondary armature typically consists of a winding and locates above the primary armature. The windings in the primary armature are electrically interconnected in series and hence the single-phase

contactless power transformer in the system has the equivalent circuit shown in Fig. 1(b). The primary armature of the single-phase systems is desired to generate the uniform magnetic field distribution along the position x . This paper discusses the planar charging system with “perpendicular flux” approach [9], in which the magnetic field generated by the primary armature links to the secondary armature perpendicularly to the surface. Therefore the magnetic field in the z -direction is considered. Fig. 1(c) shows the magnetic flux density B_z in the z -direction at $z = z_0$. The level of the uniform distribution varies sinusoidally in time and moreover in accordance with the following primary current i_1 :

$$i_1 = I_p \sin(\omega t) \quad (1)$$

where I_p is the amplitude of the current, ω is the angular frequency and t is the time. Therefore, the desired perpendicular magnetic flux density at any position of x can be expressed as follows:

$$B_z(t, x) = B_{zp} \sin(\omega t) \quad (2)$$

where B_{zp} is the amplitude of the magnetic flux density. Consequently, even if the secondary armature moves along the primary armature, it can receive constant power from the primary armature due to the magnetic field.

Fig. 2(a) illustrates a three-phase planar contactless charging system. In the primary armature, multiple sets of the three-phase windings, U_1 , V_1 and W_1 are arranged with the regular order. In the secondary armature, a set of three-phase windings is arranged in the same order as the primary windings. Fig. 2(b) shows the equivalent circuit of the three-phase contactless power transformer. The phase windings, which are the windings electrically interconnected every phase, are interconnected in wye-connection in the each armature. Fig. 2(c) shows the magnetic flux density distribution and the time-varying waveform of the magnetic flux density for the three-phase systems. In contrast to the single-phase systems, the three-phase system is desired to generate the sinusoidal distribution. Moreover, the sinusoidal distribution moves with stable amplitude when the following three-phase currents, i_{u1} , i_{v1} and i_{w1} flow in the primary windings.

$$\begin{aligned} i_{u1} &= I_p \sin(\omega t) \\ i_{v1} &= I_p \sin\left(\omega t - \frac{2}{3}\pi\right). \\ i_{w1} &= I_p \sin\left(\omega t - \frac{4}{3}\pi\right) \end{aligned} \quad (3)$$

The magnetic field moves toward x -direction as the angle ωt increases. When the angle ωt changes from 0 to 2π , the magnetic field moves by 2τ , where τ is the pole pitch, that is, 2τ is the x -direction interval length of a set of three-phase

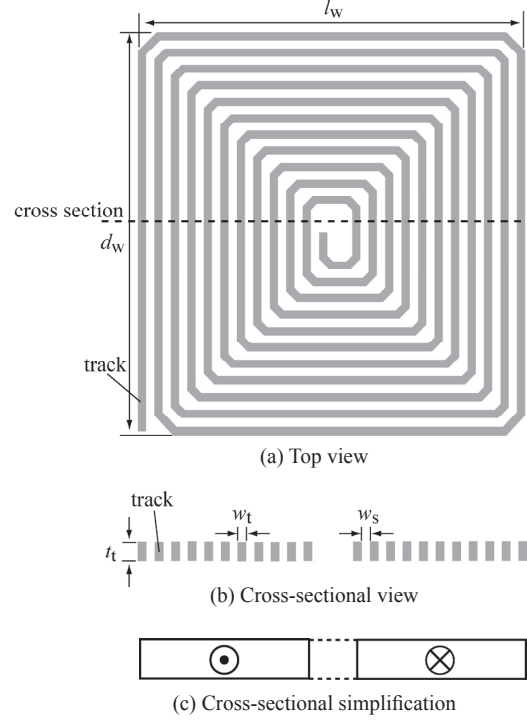


Fig.3 Structure of winding

Table I. Properties of winding

Track width, w_t	0.35 mm
Minimum space width between tracks, w_s	0.35 mm
Track thickness, t_t	0.205 mm
Winding length, l_w	16.45 mm
Winding depth, d_w	17.15 mm

windings. Therefore, the distribution at $\omega t = 2\pi$ becomes the same as that at $\omega t = 0$. Due to the moving magnetic field, the magnetic field at $x = x_0$ varies sinusoidally in the angle ωt as shown in Fig. 2(c). Similarly, at any position of x , the sinusoidal waveform of the magnetic field is produced with the phase shift by $\pi x/\tau$. Therefore, the magnetic flux density can be expressed as follows:

$$B(t, x) = B_{zp} \sin\left(\omega t - \frac{x}{\tau}\pi\right). \quad (4)$$

Consequently, the moving magnetic field also allows the three-phase system to transfer stable power regardless of the position of the secondary armature, similarly in the single-phase system.

B. Windings and their arrangement for three-phase system

In a similar manner to the single-phase system, the three-phase system employs spiral windings. Fig. 3 shows the structure of the winding. Table I gives the properties of the winding. The winding has a square shape and the number

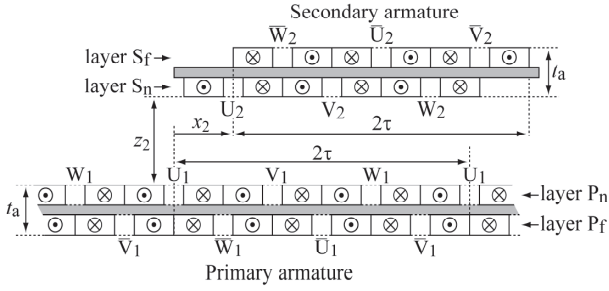


Fig. 4 Proposed arrangement

Table II Properties of armatures

Thickness of armatures, t_a	1.80 mm
Space length between windings, l_s	1.05 mm
Pole pitch, τ	26.25 mm

of turns is 11. To obtain as many turns as possible, the width of the track and the space width between the tracks are designed at 0.35 mm, which is the narrowest width in the PCB covered with copper foil with a thickness of 0.205 mm. The cross-section of this spiral winding is simplified for clear explanation, as shown in Fig. 3(c). Fig. 4 illustrates the proposed arrangement of the windings for three-phase system. This arrangement has the double layers in each armature. In the primary armature, the winding array in the layer P_f is shifted by τ in x -direction with respect to that in the layer P_n . The phase windings \bar{U}_1 , \bar{V}_1 and \bar{W}_1 in the layer P_f are electrically connected with the corresponding phase windings U_1 , V_1 and W_1 in the layer P_n as the current in the phase windings in the layer P_n flows oppositely to that in the layer P_f . In a similar manner, the secondary armature has the layer S_n and the layer S_f shifted by τ with respect to that in the layer S_n . In addition, the phase windings in the layers S_n and S_f are electrically connected oppositely with each other. Table II gives the properties of the armatures. To ensure the isolation between the different phases, a distance of 1.05 mm is spaced between the windings. Please notice that this space is omitted in Fig. 4. The resulting pole pitch τ is 26.25 mm. Therefore, the interval length 2τ of a set of the three-phase windings approximately corresponds with the length of a size AA battery or a size C battery, which are often used as a power storage device for the movers.

C. Principle to generate moving magnetic field

The principle for the primary armature to generate the moving magnetic field in the three-phase system is discussed in the subsequence explanation. Fig. 5 illustrates the simplified magnetic field flows and the distribution of B_z approximated in square wave for convenience, at $\omega t = \pi/2$ at a position of

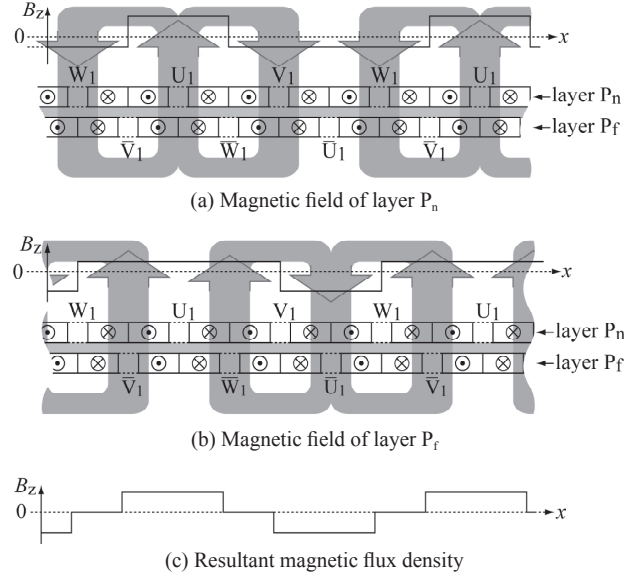


Fig.5 Magnetic field of primary armature

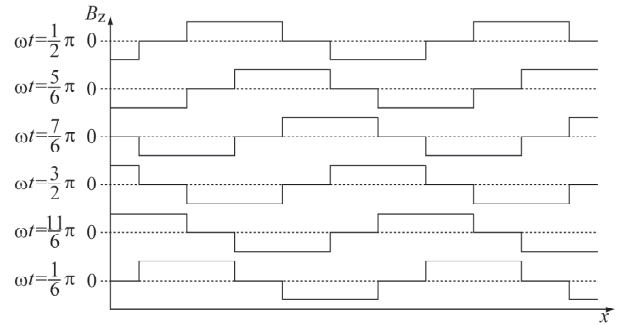


Fig.6 Moving magnetic field

z above the primary armature. Fig. 5(a) shows the magnetic field flow of the layer P_n . Above the phase winding U_1 in the layer P_n , the flow goes toward z -direction. In contrast, above the phase windings V_1 and W_1 in the layer P_n , the flow goes toward the opposite z -direction. Similarly, in terms of the magnetic field flow of the layer P_f , where the currents flow in the opposite direction from the currents in the layer P_n , the magnetic field flow has the opposite z -direction above the phase winding U_1 in the layer P_f and the z -direction above the phase windings V_1 and W_1 in the layer P_f . Consequently, these magnetic fields are superimposed each other and therefore the resultant magnetic flux density distribution is shown in Fig. 5(c). The magnetic field can become an alternating distribution. Fig. 6 illustrates the distribution of the magnetic flux densities at $\omega t = 5\pi/6, 7\pi/6, 3\pi/2, 11\pi/6$ and $\pi/6$. This result proves that the proposed arrangement for three-phase system can generate the alternating magnetic field moving toward x -direction.

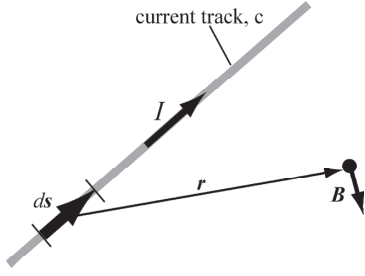


Fig. 7 Bio-Savart's Law

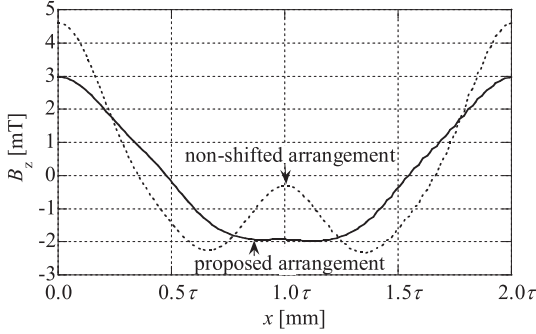
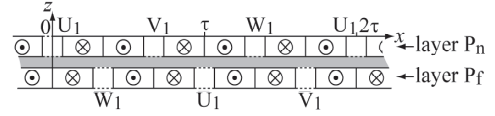
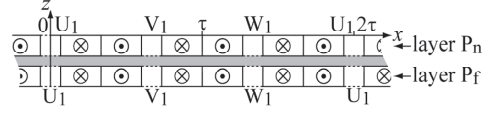


Fig. 8 Comparison of magnetic flux density distribution



(a) proposed arrangement



(b) non-shifted arrangement

Fig. 9 Arrangements of primary armature

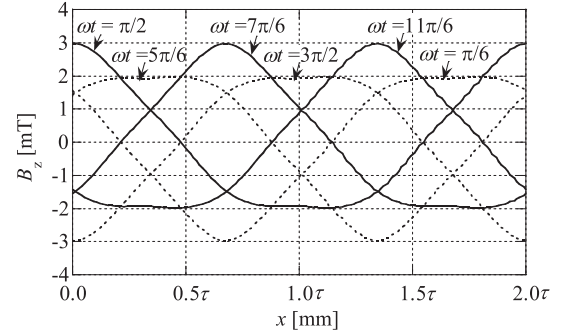


Fig.10 Magnetic flux density distribution

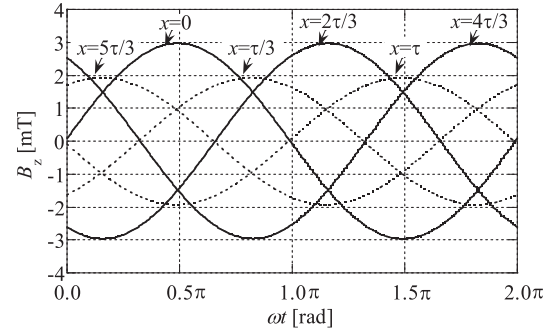


Fig.11 Magnetic flux density waveform

III. SIMULATION

The magnetic field distribution in the three-phase system is simulated. For simplicity, Both the primary and secondary armatures are assumed not to use any magnetic materials. The assumption allows the use of Bio-Savart's Law. According to the law, the magnetic flux density \mathbf{B} at a position \mathbf{r} is given by the following equation:

$$\mathbf{B} = \frac{\mu_0 I}{4\pi} \int_c \frac{d\mathbf{s} \times \mathbf{r}}{|\mathbf{r}|^3} \quad (5)$$

where the constant μ_0 is the magnetic permeability of air and the vector $d\mathbf{s}$ is the infinitesimal vector along the track c , in which the current I flows, as shown in Fig. 7. In this case, the current track c denotes the tracks of the windings in the primary armature.

Fig. 8 shows the simulated magnetic flux density distribution at $z = 4$ mm above the line, $y = 0$, which is through the centers of the windings, at $\omega t = \pi/2$. In order to compare with the result of the proposed arrangement (Fig. 9(a)), Fig. 8 contains the result of the arrangement with the winding array non-shifted between the layers P_n and P_b , shown in Fig. 9(b). The armature with non-shifted arrangement has the larger peak of the magnitude of the magnetic flux density than the armature with the proposed arrangement. The armature with non-shifted arrangement, however, has the undesirable valley of the magnitude at $x = \tau$, which is a boundary between the phase windings V_1 and W_1 . This implies that the sufficient

magnetic field is unavailable near the boundaries between phase windings. Similarly, an armature with single layer is considered to have such a valley at the boundaries as well. In contrast, the armature with the proposed arrangement can cancel the valley because the position with the valley of the magnetic field generated by one layer corresponds with that of the peak of the magnetic field generated by another layer. This result proves that the proposed arrangement can effectively improve the magnetic field distribution.

When the angle ωt changes, the magnetic flux density distribution varies as shown in Fig. 10. The magnetic field moves toward x -direction with the sufficiently large amplitude at any time and the alternating distribution, which does not contain undesired valley such as the armature with the non-shifted arrangement has. Hence, as shown in Fig. 11, the time-varying waveforms of the magnetic flux density with different x become the sinusoidal wave with the sufficiently large

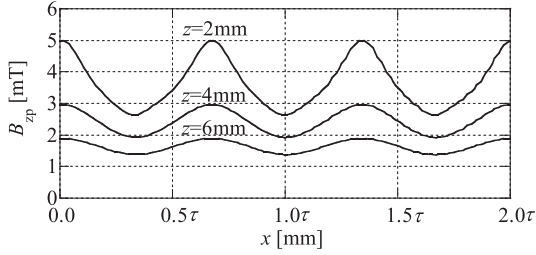


Fig.12 Amplitude of waveform of magnetic flux density

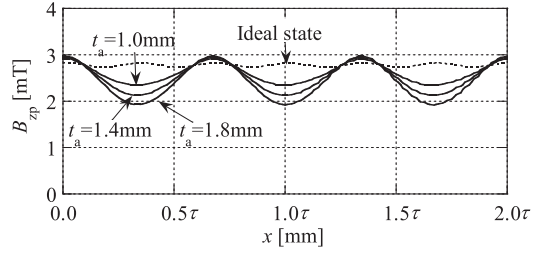


Fig.13 Amplitude of waveform of magnetic flux density, depending on t_a

amplitude. Fig. 12 shows the x -dependence of the amplitude of the waveform of the magnetic flux density. This figure describes that the sufficiently large amplitude is available at any position of x . These results bring the expectation of the sufficiently stable power transfer independent of the position of the secondary armature to the three-phase system. Moreover, in order to achieve more stable performance, it is necessary to suppress the x -depending variation of the amplitude. This variation is caused by the thickness, t_a of the armature because the layer P_1 is $(1.8 - 0.205 \approx) 1.6$ mm farther than the layer P_n from $z = 4$ mm. The variation depending on t_a can be confirmed from Fig. 13, which shows that the variation is suppressed as the thickness becomes smaller. Eventually, the variation becomes an ignorable value when the two layers overlap completely as an ideal state, which is practically unfeasible. On the other hand, the increase in z also suppresses the variation according to Fig. 12.

IV. EXPERIMENT

Fig. 14 shows the experimental circuit configuration for the three-phase system. This system consists of the three-leg inverter fed by DC voltage source, two groups of the capacitors and the resistive load. The three-leg inverter generates three-phase ac voltages under the switching patterns shown in Fig.15. The switches are turned on in a duty cycle of 50%. In addition, the on-timings of the switches on the each leg are shifted by $2\pi/3$, each other. The output terminals of the inverter are connected through a group of the capacitors C_1 , with the primary armature of the three-phase contactless power transformer illustrated in Fig. 2(b). The secondary

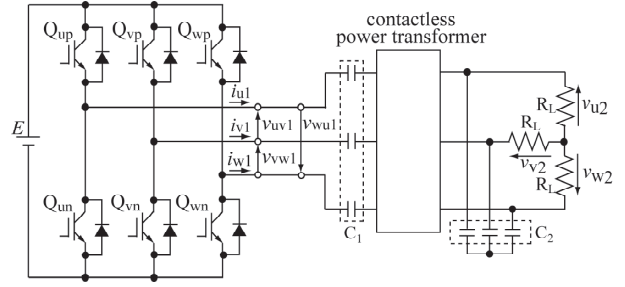


Fig. 14 Experimental circuit configuration

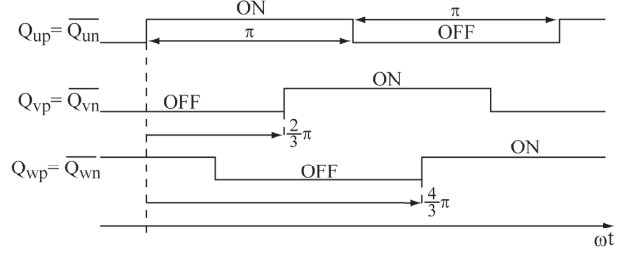


Fig. 15 Switching patterns for inverter

Table III Inductance values of prototype transformer

L_{u1}	6.95 [μ H]
L_{v1}	6.92 [μ H]
L_{w1}	6.97 [μ H]
L_{u2}	2.31 [μ H]
L_{v2}	2.31 [μ H]
L_{w2}	2.31 [μ H]

armature is connected with another group of the capacitors C_2 and the load. The capacitors and the inductors in the contactless power transformer constitute resonant circuits. In a similar manner to the single-phase systems, there is a choice of series or parallel resonant circuit, in the three-phase system [5]. In this paper, the group of C_1 is connected in series and the group of C_2 is connected in parallel with the inductors. The values of the capacitors are determined as follows:

$$C_1 = \frac{1}{L_1(2\pi f)^2} \tag{6}$$

$$C_2 = \frac{1}{L_2(2\pi f)^2} \tag{7}$$

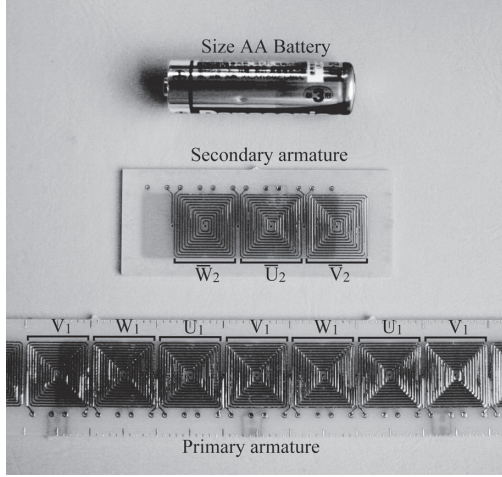
where f is the resonant frequency, which also is the switching frequency of the inverter and is given by the following equation:

$$f = \frac{\omega}{2\pi}. \tag{8}$$

The values L_1 and L_2 of the inductance represent the average values of the primary inductance, L_{u1} , L_{v1} and L_{w1} and the

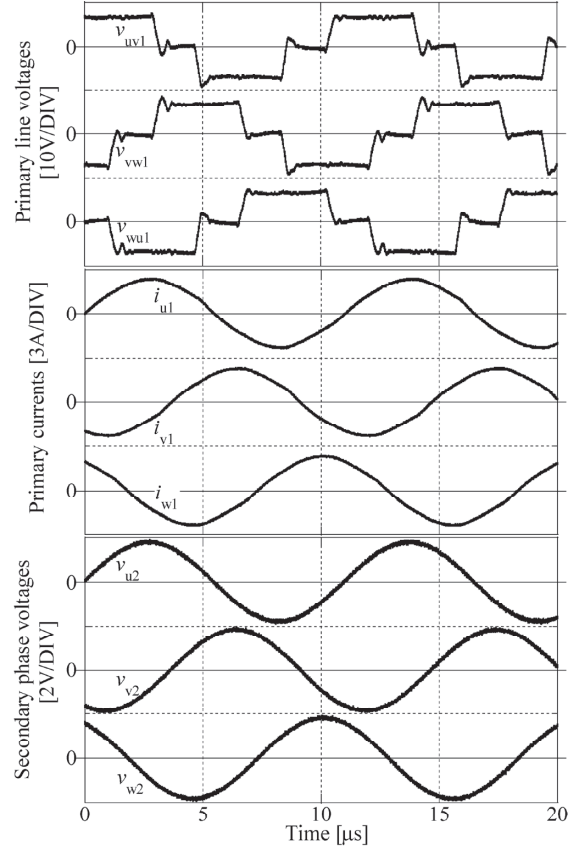
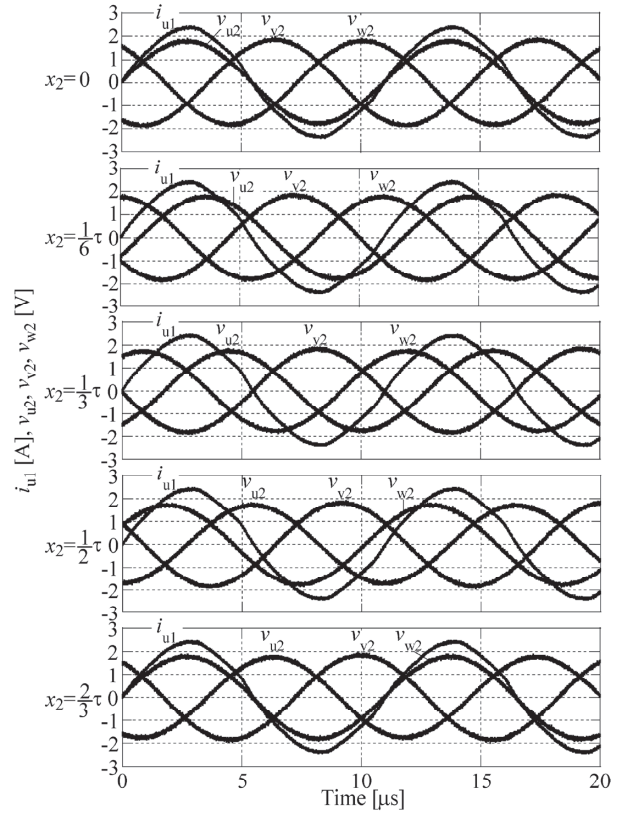
Table IV Experimental conditions

DC source voltage, E	8.6 [V]
Resonant frequency, f	91 [kHz]
Primary resonant capacitance, C_1	0.36 [μ F]
Secondary resonant capacitance, C_2	1.10 [μ F]
Load resistance, R_L	5.1 [Ω]

**Fig. 16** Prototype of three-phase contactless power transformer

secondary inductance, L_{u2} , L_{v2} and L_{w2} , of the prototype for the experiments, respectively. These values are given by Table III. Fig. 16 shows the prototype of the three-phase contactless power transformer. This has the proposed arrangement of the windings and the properties in Tables I and II. Table IV shows the experimental conditions, which include C_1 and C_2 calculated from (6) and (7).

Fig. 17 shows the experimental waveforms at $x_2 = 0$ and $z_2 = 3$ mm, where x_2 and z_2 are x - and z -direction positions of the secondary armature, respectively, defined in Fig. 4. Although the primary line voltages, v_{uv1} , v_{vw1} and v_{wu1} have the square waveforms, the primary currents, i_{u1} , i_{v1} and i_{w1} have the sinusoidal waveforms with resonant frequency f , due to the resonant circuit. The resulting secondary phase voltages, v_{u2} , v_{v2} and v_{w2} are balanced, that is, they have the sinusoidal waveforms with the same amplitude values of approximately 2.0 V and are shifted by $\omega t = 2\pi/3$ each other. Fig. 18 shows the secondary phase voltages with different x_2 . At $x_2 = 0$, the voltage v_{u2} is in phase with i_{u1} and the other phase voltages, v_{v2} and v_{w2} shift by $2\pi/3$ and $4\pi/3$ with respect to i_{u1} , respectively. As the secondary armature moves toward x -direction, the voltages lag behind i_{u1} and at $x_2 = 2\tau/3$, the voltages shift by $2\pi/3$ respectively, as a result, v_{w2} becomes in phase with

**Fig. 17** Waveforms at $x_2 = 0$ and $z_2 = 3$ mm**Fig. 18** Secondary phase voltages with different x_2

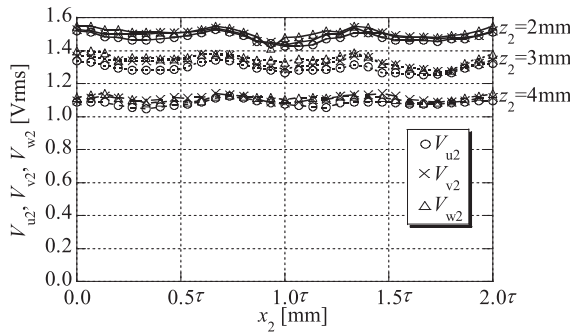


Fig. 19 Secondary phase voltages

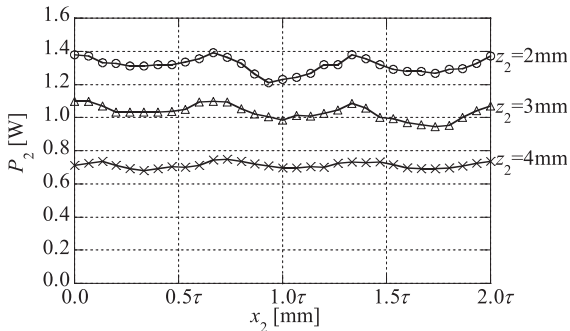


Fig. 20 Transferred power

i_{u1} . Moreover, these results describe that the amplitudes are maintained at approximately 2.0V in spite of the movement of the secondary armature. Fig. 19 shows the x_2 -dependence of the rms values V_{u2} , V_{v2} and V_{w2} of the secondary phase voltages. These voltages are maintained near constant, which leads the stable performance to the three-phase system in any position of x_2 . According to Fig. 20, the total power P_2 transferred to the secondary armature is approximately 0.7, 1.0 and 1.3W at $z_2=4, 3$ and 2 mm, respectively. In addition, the ripple of P_2 , which is caused by the ripple of the magnetic field shown in Fig. 12 can be suppressed sufficiently.

V. CONCLUSIONS

The planar contactless charging system applying the three-phase power transformer has been proposed. The operation principle, which is different from that of the conventional planar contactless charging systems with the single-phase power transformer, has been explained. For the three-phase system, the arrangement of the windings has been proposed. The principle of the three-phase system requires that the magnetic field moves with the stable amplitude at any time, in order to realize the stable power transfer. The simulations confirm that the moving magnetic field generated by the primary armature with the proposed arrangements satisfies the principle. Consequently, the experiments confirm that the prototype with the arrangement can transfer sufficient

and stable power regardless of the position of the secondary armature.

Future works shall deal with the suggestions of the arrangement of the windings in order to achieve the smaller ripple of the transferred power and moreover the optimal value of the capacitances for the three-phase resonant circuits, considering the mutual inductance between the phases.

REFERENCES

- [1] C. S. Wang, O. H. Stielau and G. A. Covic, " Design Considerations for a Contactless Electric Vehicle Battery Charger", *IEEE Trans. Ind. Electron.*, vol.52, no.5, pp.1308-1314, Oct., 2005.
- [2] J. Sallan, J. L. Villa A. Llombart and J. F. Sanz, " Optimal Design of ICPT Systems Applied to Electric Vehicle Battery Charge", *IEEE Trans Ind. Electron.*, vol.56, no.6, pp.2140-2149, Jun., 2009.
- [3] U. K. Madawala, D. J. Thrimawithana and N. Kularatna "An ICPT-Supercapacitor Hybrid System for Surge-Free Power Transfer", *IEEE Trans. Ind. Electron.*, vol.54, no.6, pp.3287-3297, Dec., 2007.
- [4] S.Y. R. Hui and W. W. C. Ho, " A New Generation of Universal Contactless Battery Charging Platform for Portable Consumer Electronic Equipment", *IEEE Trans. Power Electron.*, vol.20, no.3, pp.620-627, May, 2005.
- [5] C. S. Wang, G. A. Covic and O. H. Stielau, " Power Transfer Capability and Bifurcation Phenomena of Loosely Coupled Inductive Power Transfer Systems", *IEEE Trans. Ind. Electron.*, vol.51, no.1, pp.148-157, Feb., 2004.
- [6] P. Sergeant and A. Van den Bossche, " Inductive coupler for contactless power transmission", *IET Electr. Power Appl.*, vol.2, no.1, pp.1-7, Jan., 2008.
- [7] G. A. Covic, J. T. Boys, M. L. G. Kissin and H. G. Lu, " A Three-Phase Inductive Power Transfer System for Roadway-Powered Vehicles", *IEEE Trans. Ind. Electron.*, vol. 54, no.6, pp.3370-3378, Dec., 2007.
- [8] X. Liu and S. Y. R. Hui, " Optimal Design of a Hybrid Winding Structure for Planar Contactless Battery Charging Platform", *IEEE Trans. Power Electron.*, vol.23, no.1, pp.455-463, Jan., 2008.
- [9] X. Liu and S. Y. R. Hui, " Equivalent Circuit Modeling of a Multilayer Planar Winding Array Structure for Use in a Universal Contactless Battery Charging Platform", *IEEE Trans. Power Electron.*, vol.22, no.1, pp.21-29, Jan., 2007
- [10] J. Achterberg, E. A. Lomonova and J. de Boeij, " Coil Array Structures Compared for Contactless Battery Charging Platform", *IEEE Trans. Magn.*, vol.44, no.5, pp.617-622, May, 2008.